A EUROPEAN JOURNAL OF CHEMICAL BIOLOGY

CHEMBIOCHEM

SYNTHETIC BIOLOGY & BIO-NANOTECHNOLOGY

Accepted Article

Title: Mechanistic Insight into the Catalytic Promiscuity of Amine Dehydrogenases: Asymmetric Synthesis of Secondary and Primary Amines

Authors: Vasilis Tseliou, Marcelo F. Masman, Wesley Böhmer, Tanja Knaus, and Francesco Mutti

To be cited as: *ChemBioChem* 10.1002/cbic.201800626

Link to VoR: http://dx.doi.org/10.1002/cbic.201800626

A Journal of ChemPubSoc Europe

WILEY-VCH

www.chembiochem.org

10.1002/cbic.201800626

Mechanistic Insight into the Catalytic Promiscuity of Amine Dehydrogenases: Asymmetric Synthesis of Secondary and Primary Amines

Vasilis Tseliou,[a] Marcelo F. Masman,[a] Wesley Böhmer,[a] Tanja Knaus,[a] and Francesco G. Mutti,[a]*

Van 't Hoff Institute for Molecular Sciences, HIMS-Biocat, University of Amsterdam, Science Park 904, 1098 XH, The Netherlands.

Corresponding Author: **f.mutti@uva.nl**

10.1002/cbic.201800626

Abstract

Biocatalytic asymmetric aminations of ketones using amine dehydrogenases (AmDHs) or transaminases, are efficient methods for the synthesis of α-chiral primary amines. A major challenge is the extension of the amination to the synthesis of secondary and tertiary amines. Herein, we show for the first time that AmDHs are capable of accepting other amine donors, hence giving access to enantioenriched secondary amines with conversions up to 43%. Surprisingly, in several cases, we observed the promiscuous formation of enantiopure primary amines along with the expected secondary amines. By conducting practical laboratory experiments and computational experiments, we propose that the promiscuous formation of primary amines along with secondary amines is due to an unprecedented nicotinamide (NAD)-dependent formal transamination catalysed by AmDHs. In nature, this type of mechanism is commonly performed by pyridoxal 5'-phosphate (PLP) aminotransferase and not by dehydrogenases. Finally, we propose a catalytic pathway that rationalises the promiscuous NAD-dependent formal transamination activity and explains the formation of the observed mixture of products. This work increases our understanding on the catalytic mechanism of NAD-dependent aminating enzymes such as AmDHs and will aid further research on the rational engineering of oxidoreductases for the synthesis of α-chiral secondary and tertiary amines.

10.1002/cbic.201800626

Introduction

Catalytic enzyme promiscuity is the ability of an enzyme to catalyse alternative chemical reactions by often following catalytic mechanisms that are different from the natural one.[1] Although catalytic enzyme promiscuity has been the object of intensive investigation for two decades, the discovery of new promiscuous activities still proceeds at regular pace as witnessed by recent publications.[2] Notably, these new biocatalytic activities have been frequently exploited in chemical synthesis.

Amine dehydrogenases (AmDHs) catalyse the reductive amination of carbonyl compounds at the expense of aqueous ammonium/ammonia buffer. All the known AmDHs so far were obtained mainly by protein engineering starting from α-amino acid dehydrogenases such as the leucine dehydrogenases from *Bacillus stereothermophilus*,[3] *Exiguobacterium sibiricum*,[4] *Lysinibacillus fusiformis*[5] and *Bacillus sphaericus*, [5] as well as the phenylalanine dehydrogenases from *Bacillus badius*,[6] *Rhodococcus* sp. M4 [7] and *Caldalkalibacillus thermarum*. [8] In all these cases, the mutations of the highly conserved lysine and asparagine residues in the active site, which interact with the two oxygen atoms of the carboxylic moiety of the natural substrate, were essential for switching the substrate specificity from α-keto carboxylic acids to ketones.[3, 6-8] A few native amine dehydrogenases have been also identified from *Petrotoga mobilis*, *Fervidobacterium nodosum*, *Clostridium sticklandii*, *Dethiosulfovibrio peptidovorans*, *Staphylothermus hellenicus*, and *Thermosediminibacter oceani*.[9] Several works on the asymmetric biocatalytic reductive amination using the above mentioned amine dehydrogenases (AmDHs) have been published very recently using isolated enzymes, immobilised enzymes or whole cells biocatalysts.[3-10] In particular, our group has shown that AmDHs are efficient catalysts for the reductive amination of prochiral ketones (i.e. TONs > 10^3) and their substrate scope covers already a respectable range of

10.1002/cbic.201800626

structurally diverse substrates.[10d] Biocatalytic reductive amination is also possible with imine reductases (IReds), which catalyse naturally the asymmetric reduction of cyclic imines.[11] In fact, during the past few years, various groups have shown that IReds are also capable of catalysing the reductive amination of non-cyclic imines although with modest efficiency.[12] In a recent study, the reductive amination between ketones and small aliphatic and benzylic amines was carried out with a novel dehydrogenase from *Aspergillus o.* (AspRedAm).[13] The enzyme was classified as a "reductive aminase (RedAm)". In a follow-up study two additional RedAms were characterised.[14] Finally, a previous patent from Codexis reported a reductive aminase activity from a library of variants originated from an opine dehydrogenase.[15]

Despite differences in names and apparent reactivity, the catalytic mechanisms of IReds, AmDHs and RedAm are closely related as the actual mechanism is essentially based on the hydride transfer from the nicotinamide coenzyme (NADH or NADPH) to the *in-situ* formed imine intermediate or the already existing cyclic imine in solution. Thus, we hypothesised that the reactivity of AmDHs may not be restricted only to ammonia as amine donor as previously believed and reviewed elsewhere.[11b] That was also suggested by a number of oxidoreductases present in nature such as the opine dehydrogenases, which are capable of generating secondary amines by the coupling of an α-amino acid with an α-keto acid.[16]

Herein, we show for the first time that the reactivity of AmDHs is indeed not limited to ammonia as the amine donor. The two AmDHs, considered in the present study, can accept other amine donors to enable the formation of secondary and tertiary amines. Surprisingly, in some cases, the reaction was accompanied by the promiscuous formation of primary amines along with the expected secondary and tertiary amines. With the aim of explaining such unprecedented promiscuous activity as well as the stereoselective outcome of the reaction, we performed a study

10.1002/cbic.201800626

based on an accurate combination between practical laboratory experiments and computational studies. Consequently, herein we also propose a catalytic cycle for amine dehydrogenases, which explains the promiscuous formation of all products (i.e. secondary and primary amines) as well as the enantiomeric composition of the reaction mixture.

Results and discussion

Screening of carbonyl compounds and amine donors. The reactivities of Rs-AmDH (originated by enzyme engineering from the phenylalanine dehydrogenases from *Rhodococcus sp.* M4)[7, 10d] and of Ch1-AmDH[10b, 10d] (a chimeric enzyme obtained via domain shuffling of first generation variants) were assayed with eleven different amine donors, which also constituted the buffer system. Four different types of carbonyl compounds were selected: aliphatic ketones, aromatic ketones, aliphatic aldehydes and aromatic aldehydes (Scheme 1; for the complete list of carbonyl compounds and amine donors, see Figure S1 and Figure S2). We conducted the initial biocatalytic reactions as follows: carbonyl compound (10 mM), amine/aminium formate buffer (1 M, pH 8.5), N-terminal His_6-tagged Rs-AmDH (>99% purity, 103 μM, 1 mol%) or N-terminal His_6-tagged Ch1-AmDH (>99% purity, 92 μM, 0.9 mol%), NAD^+ (1 mM) and N-terminal His_6-tagged Cb-FDH (>99% purity, 24 μM, 0.2 mol%; for recycling of NADH), at ambient temperature, for 48 h.

10.1002/cbic.201800626

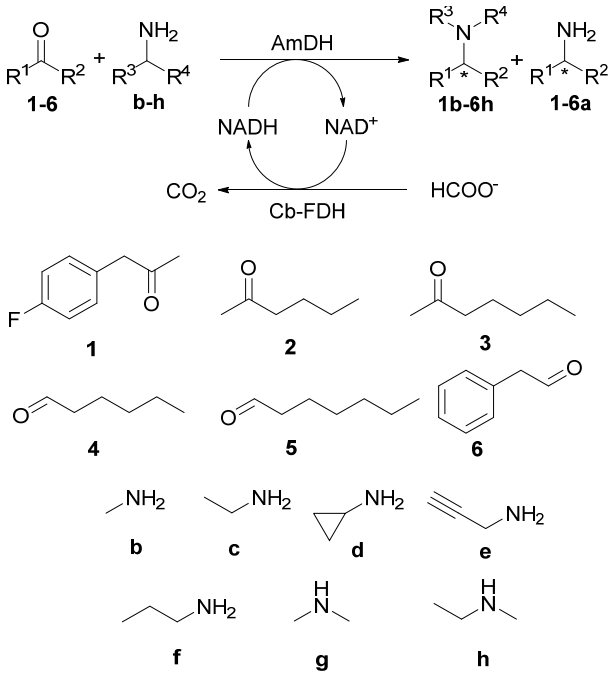

Scheme 1 Biocatalytic reductive amination of carbonyl compounds (**1-6**, 10 mM) with different amine donors (**b-h**) catalysed by N-terminal His_6-tagged amine dehydrogenases (AmDHs). The amine donor was also used as buffer species in water for the reaction (1 M, pH 8.5, formate as counter-anion). The nicotinamide coenzyme (NAD^+, 1 mM) was recycled by reduction with formate, which is catalysed by N-terminal His_6-tagged formate dehydrogenase from *Candida boidinii* (Cb-FDH). The amination reaction generated the following secondary or tertiary amines (**1b-d**, **2b**, **3b**, **4b**, **5e**, **6b-c**, **6f-h**) along with the unexpected formation of the following structurally related primary amines (**1-3a**). For full experimental screening, see SI, Table S1.

Under the mentioned reactions conditions, both tested AmDHs produced secondary or tertiary amines starting from ketones and aldehydes (for complete list of products, see Figure S3). Selected results are reported in Table 1, whereas all screening results are reported in SI section 4 (Table S1). Ch1-AmDH catalysed the reductive amination between 4'-fluorophenylacetone (**1**) and methylamine (**b**), whereas Rs-PhAmDH accepted ketone **1** in combination with ethylamine (**c**) and cyclopropylamine (**d**) (Table 1, entries 1, 3, 4). For these reactions, we were surprised to identify also the formation of the structurally related

10.1002/cbic.201800626

primary amine, 4'-fluoroamphetamine (**1a**), as a second product. Notably, **1a** was obtained in enantiopure form in all the cases (*ee* > 99%, *R*). Commercial reagent grade solution of methylamine contains only negligible traces of ammonia, whereas ethylamine and cyclopropylamine do not contain ammonia at all. In addition, the amination of **1** at 4-6 M concentration of methylamine buffer (**b**) resulted in lower conversion into **1a** compared to the same reaction performed at 3 M of **b** (Figure 1B). Hence, we ruled out the possibility that the primary amine could have been formed via the enzymatic reaction between the ketone and the ammonia present, eventually, as an impurity. Due to the complexity and the elevated polarity of the components in the reaction mixtures, we succeeded in measuring the enantiomeric excess of the secondary amine products by chromatography in the case of compounds **1b** and **1d**. **1b** was obtained in enantioenriched form (*ee* 72% *R*, Table 1, entry 1), whereas **1d** in nearly racemic form (Table 1, entry 4). In contrast, the other product - primary amine **1a** - was obtained in enantiopure form as previously observed (for comparison, Table 1, entries 1 and 4).

Ch1-AmDH was the most active enzyme for the amination of 2-hexanone (**2**) and 2-heptanone (**3**) with **b** (Table 1, entries 5 and 6). Even in this case, the structurally related primary amines 2-aminohexane (**2a**) and 2-aminoheptane (**3a**) were obtained with perfect *ee*. These results confirm that the formation of primary amines occurs during the catalytic cycle of the AmDHs. Conversely, the amination of aldehydes using the AmDHs and different amine donors under our initial reaction conditions (1 M of amine/aminium buffer, pH 8.5), proceeded with perfect chemoselectivity to afford the expected secondary amines as the sole product up to 43% conversion (Table 1, entry 7-11). As a proof of principle, the amination was run also with secondary amines as amine donor (*e.g.* dimethylamine, ethyl-

10.1002/cbic.201800626

methylamine), leading to tertiary amines albeit with poor conversions (Table 1, entry 12 and 13).

Table 1. Reductive amination reactions performed by AmDHs for the synthesis of secondary and tertiary amines. Standard reaction conditions: substrate (10 mM), N-terminal His6-tagged Ch1-AmDH (>99% purity, 92 μM, 0.9 mol%) or N-terminal His6-tagged Rs-AmDH (>99% purity, 103 μM, 1 mol%), N-terminal His6-tagged Cb-FDH (>99% purity, 24 μM, 0.2 mol%) and buffer constituted by amine donor with formate as counter-anion (1 M, pH 8.5). The reactions were performed at 30 °C, for 48 h using an orbital shaker at 170 rpm.

Entry	Substrate	Amine donor	AmDH	Secondary Amine		Primary Amine (1-11a)	
				Conv. (%) [b]	*ee* (%) [c]	Conv. (%) [b]	*ee* (%) [c]
1	**1**	**b**	Ch1	15	72 (*R*)	8.	>99 *(R)*
2	**1**	**b**	Ch1	40 [a]	64 (*R)*	6	>99 *(R)*
3	**1**	**c**	Rs	4	N.m.	26	>99 *(R)*
4	**1**	**d**	Rs	11	1 (*R*)	26	>99 *(R)*
5	**2**	**b**	Ch1	5	N.m.	4	>92 *(R)* [d]
6	**3**	**b**	Ch1	32	N.m.	26	>99 *(R)*
7	**4**	**b**	Rs	24	N.a.	N.d.	N.a.
8	**5**	**e**	Ch1	41	N.a.	N.d	N.a.
9	**6**	**b**	Rs	29	N.a.	N.d	N.a.
10	**6**	**c**	Rs	40	N.a.	N.d	N.a.
11	**6**	**f**	Rs	43	N.a.	N.d	N.a.
12	**6**	**g**	Rs	3 [e]	N.a.	N.d	N.a.
13	**6**	**h**	Rs	8 [e]	N.a.	N.d	N.a.

[a] Concentration of $MeNH_2/MeNH_3^+$ buffer was increased to 6 M. [b,c] For analytical determination of conversions and *ee*s, see SI paragraphs 8-10. [d] Unable to determine with precision, due to experimental noise of the GC traces. [e] Measured by GC-MS.

10.1002/cbic.201800626

Influence of the enzyme and amine donor concentration. For further studies, we selected the amination of 4'-fluorophenylacetone (**1**) with methylamine (**b**) as test reaction. In the first set of experiments, we kept the buffer concentration constant (1 M, pH 8.5) and we varied the concentration of N-terminal His_6-tagged Ch1-AmDH (>99% purity, 4.5–91 μM, equal to 0.045-0.9 mol%). As expected, increasing the enzyme concentration affected positively the overall conversion (Figure 1A, Table S2). Interestingly, the ratio between the formation of secondary (**1b**) and primary (**1a**) amines also varied depending on the enzyme concentration from 1:1.2 (at AmDH 4.5 μM) to 1:1.9 (at AmDH 91 μM).

In a follow-up experiment (Figure 1B), we fixed the concentration of N-terminal His_6-tagged Ch1-AmDH (>99% purity, 91 μM, 0.9 mol%) and we increased the concentration of the $CH_3NH_2/CH_3NH_3^+$ buffer (200 mM – 6 M). Increasing the buffer concentration correlated with a consistent increase in the formation of **1b**. At 6 M buffer concentration, **1b** was finally obtained in 40% conversion (Figure 1B and Table 1 entry 2; for details see SI, Table S3). The side-reaction that leads to the primary amine product showed a continuous increment of conversion of **1a** (11% conversion) up to a buffer concentration of 3 M. Surprisingly, more elevated concentration of buffer (4, 5, 6 M) reduced the formation of **1a** (6% at 6 M buffer concentration). Hence, the ratio between **1a** and **1b** further increased to 1:6.6. We also monitored a possible variation in the stereoselective outcome of the reaction. The enantiomeric excess of the secondary amine product **1b** was partially affected with a reduction from 72% *ee* (1 M buffer) to 64% *ee* (6 M buffer). In contrast, the optical purity of the primary amine remained perfect (>99%, Table 1 entries 1 and 2). In all cases, the *R*-configured amine (secondary or primary) was the favoured enantiomer.

10.1002/cbic.201800626

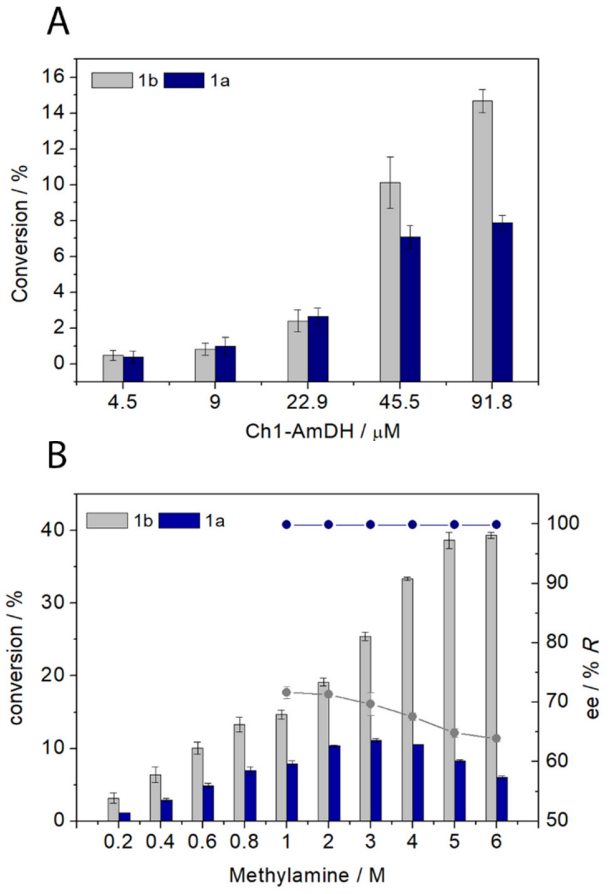

Figure 1. (A) Dependence of enzyme concentration (>99% purity, 4.5-91 µM, equal to 0.045-0.9 mol%) at fixed concentrations of methylamine buffer (1 M) for the conversion of 4'-fluorophenylacetone (**1**) into primary (**1a**, blue columns) and secondary (**1b**, grey columns) amines catalysed by N-terminal His_6-tagged Ch1-AmDH. Catalytic amount of NAD^+ (1 mM) was applied and recycled using N-terminal His_6-tagged Cb-FDH (>99% purity, 24 µM, 0.2 mol%). Error bars represent the standard deviation calculated from three independent experiments. **(B)** Dependence of CH_3NH_2 concentration (200 mM - 6M) at a fixed concentration of N-terminal His_6-tagged Ch1-AmDH (>99% purity, 91 µM, 0.9 mol%) for the conversion of 4'-fluorophenylacetone (**1**) into primary (**1a**, purple columns) and secondary (**1b**, grey columns) amines catalysed by Ch1-AmDH. Catalytic amount of NAD^+ (1mM) was applied and recycled using N-terminal His_6-tagged Cb-FDH (>99% purity, 24 µM, 0.2 mol%). Error bars represent the standard deviation from three independent experiments. Enantiomeric excess (ee) for **1a** (blue) and **1b** (grey) are depicted with circles connected with a solid line.

10.1002/cbic.201800626

Initial biochemical and computational studies towards the understanding of the reaction mechanism. Both Ch1-AmDH and Rs-AmDH showed to possess a general perfect stereoselectivity (i.e. "*R*-selectivity") for the reductive amination of prochiral ketones with ammonia.[10d] However, different points remained unclear at this stage: 1) the molecular discriminants that determine a productive combination between the ketone/aldehyde and the amine donor; 2) the formation of secondary amines with moderate steroselectivity; 3) the unexpected formation of primary amine in enantiopure form.

Therefore, we performed several computational analysis in the attempt of elucidating these points. First, we generated several models of Rs-AmDH in complex with NADH and different protonated imine intermediates (*i.e.* carbonyl compounds: 4'-fluorophenylacetone (**1**), hexanal (**4**), heptanal (**5**), phenylacetaldehyde (**6**), 4-phenyl-butan-2-one (**9**), acetophenone (**10**); amine donors: ammonia (**a**), methylamine (**b**), ethylamine (**c**) and *n*-propylamine (**f**)). Details on the creation of these models are reported in the experimental section. Based on the reported catalytic mechanism of the parent wild-type phenylalanine dehydrogenase from *Rhodococcus sp.* M4,[17] we analysed the models considering two crucial parameters as depicted in Figure 2: 1) the distance between the departing hydride of NADH and the prochiral carbon of the imine intermediate (herein referred as "distance 1"); 2) the distance between the negatively charged oxygen atom of the terminal carboxylic group of Asp118 of Rs-AmDH and the hydrogen of the positively charged iminium group of the intermediate (herein referred as "distance 2").

10.1002/cbic.201800626

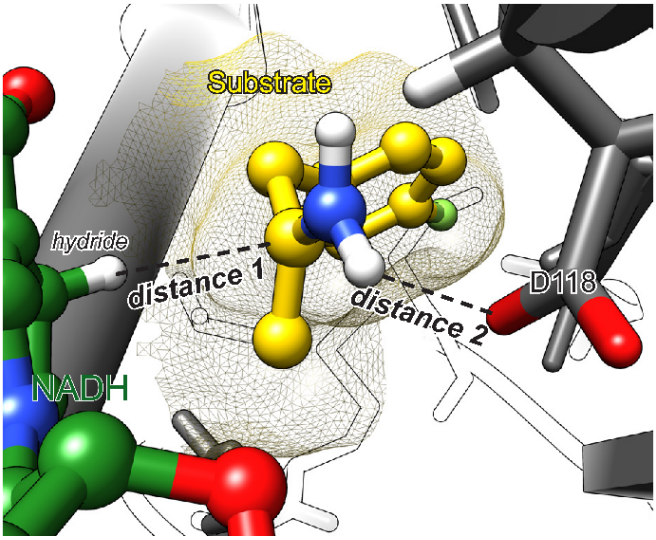

Figure 2. Simplified schematic view of the productive binding mode for the iminium intermediate bound in the active site of the AmDH. For clarity, only the nicotinamide coenzyme in its reduced form (NADH) and the highly conserved amino acid residue Asp 118 (numbering of Rs-AmDH) of the enzyme are depicted. The actual spatial positions and orientations of NADH, substrate and Asp 118 in the active site were retained according to our calculated model. The iminium intermediate (**1a***) is depicted. **1a*** is generated by interaction between 4'-fluorophenylacetone (**1**) and ammonia (**a**). The crucial distances 1 and 2 are depicted with a solid black line.

Our analysis revealed that highest reactivity (*i.e.* conversion) for the reductive amination is achieved when both above-mentioned distances have an optimal value. The sum of the van der Waal's radius [18] of carbon and hydrogen can be considered as the threshold distance, which is ca. 2.9 Å ($r_H^{vdw} = 1.2$ Å, $r_C^{vdw} = 1.7$ Å; for details see experimental part). Thus, an optimal distance must be around or moderately below 2.9 Å. For instance, the reductive amination of **1** with ammonia (**a**) catalysed by Rs-AmDH was reported to proceed quickly and in quantitative manner.[10d] Our model for this reaction with Rs-AmDH and the related iminium intermediate (**1a***) displays indeed an optimal "distance 1" of 2.7 Å and an optimal "distance 2" of 1.9 Å (see SI, Figure S5A). Conversely, the same reaction between **1** and

10.1002/cbic.201800626

ethylamine (**c**) affords only 4% conversion (Table 1, entry 3). In our models for the latter reaction considering the related iminium intermediate **1c***, the "distance 1" is still ideal (2.9 - 3.0 Å), whereas the "distance 2" is significantly larger (4.8 - 6.0 Å), (see SI, Figure S5B and S5C). Another interesting example is the reductive amination between acetophenone (**10**) and either ammonia (**a**) or ethylamine (**b**). The reaction with ammonia (**a**) as amine donor afforded only a moderate conversion of 34% after 48 h;[10d] our model for this reaction with the related iminium intermediate **10a*** (see SI, Figure S5D) displays an optimal "distance 1" of 3.0 Å, but "distance 2" is slightly elongated (3.3 Å). Conversely, the reaction between acetophenone (**10**) and ethylamine (**b**) did not occur at all (see SI Table S1); in fact, although one of our models for this reaction with iminium intermediate **10b*** displays an optimal "distance 2" of 3.00 Å, "distance 1" is much larger (4.0 Å; see SI, Figure S5E). Finally, 4-Phenyl-butan-2-one (**9**) and ammonia (**a**) react quantitatively within short reaction time.[7, 10d] Our model for this reaction with iminium intermediate **9a*** shows both perfect "distance 1" and "distance 2" of 2.8 Å and 3 Å, respectively (see SI Figure S5G). In contrast, the reaction between 4-phenyl-butan-2-one (**9**) and ethylamine (**b**) did not occur. Coherently, our models for this reaction with iminium intermediate **9b*** show a longer "distance 1" ranging from 3.4 Å and 3.5 Å (see SI, Figure S5H and S5I). A similar study conducted with aldimine as intermediates provided an analogous trend (see SI, Figure S6). In conclusion, our analysis revealed that the distance between the prochiral iminium carbon of the intermediate and the hydride of NADH (Figure 2, distance 1) is the parameter of primary importance for the reaction to occur. Nevertheless, the residue Asp118 (numbering of Rs-AmDH) appears to play a role for achieving relevant turnovers (Figure 2, distance 2). However, this analysis permits only to rationalise which are the

10.1002/cbic.201800626

crucial parameters that enable the reduction of the iminium intermediate bound in the active site of an AmDH. Otherwise, the reductive amination of a prochiral ketone with different amine donors (**b-e**) catalysed by AmDHs generates complex reaction mixtures containing secondary amines (**1b-d**, **2b**, **3b**, **4b**, **5e**) with moderate optical purity and the unexpected primary amines in enantiopure form (**1-3a**). This observation suggests the existence of, at least, two stereocomplementary productive binding configurations for the reduction of secondary iminium intermediates.

On the other hand, as the unexpected primary amines (**1-3a**) were always obtained in optically pure form (>99% ee, *R*), the promiscuous formation of these products was clearly catalysed by the AmDHs. At this stage, we envisioned three possible reaction mechanisms that could explain the formation of primary amines (Scheme 2).

The first option (Scheme 2a) foresees an oxidative deamination of the amine donor (**b-d**; **d** in the example), which is catalysed by the AmDH. The free ammonia generated in the first step may serve as the amino donor in a subsequent reductive amination that is always catalysed by the AmDH. The second option (Scheme 2b) for explaining the formation of the enantiopure primary amine as side-product foresees an unlikely promiscuous hydrolytic activity of AmDHs. In fact, a polarised water molecule in the active site of AmDH and possessing a proper orientation, may attack the sp^3-carbon in α-position to the nitrogen of the ketiminium intermediate (**1d*** in the example). Although such a hydrolytic step is chemically unlikely, it cannot be excluded beforehand because of the particular catalytic environment in the active site of the AmDH in which a polarised water molecule is normally involved in catalysis.[17] If such a hydrolytic step occurred, a subsequent hydride transfer from NADH would generate a primary amine. Furthermore, only in the case of cyclic

10.1002/cbic.201800626

intermediates such as **1d***, the same nucleophilic attack of a water molecule may also provoke the opening of the cyclopropyl ring to give an aminol upon reduction (not depicted in Scheme 2b). However, this route is also incompatible with the observed mixture of products. The third option (Scheme 2c) is an unprecedented formal transamination reaction. In nature, transamination reactions are catalysed by pyridoxal 5'-phosphate (PLP) dependent aminotransferase through a ping-pong mechanism.[19] However, an alternative NAD^+/NADH redox-mediated mechanisms is conceivable. According to this hypothesis, the key catalytic step would be the isomerisation of the ketiminium intermediate (**1d*** in the scheme 2c) by the action of NAD^+/NADH, to give the other ketiminium intermediate **1d****.

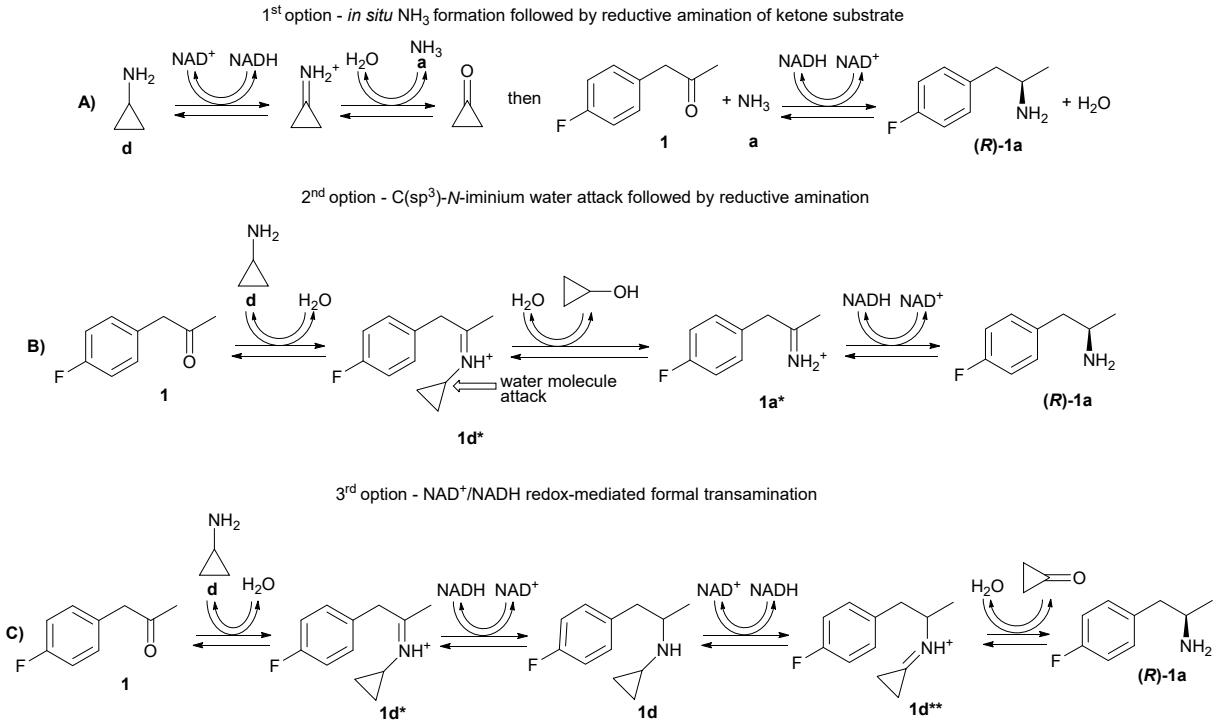

Scheme 2. Possible mechanistic explanations for the promiscuous formation of enantiopure primary amine as by-product.

10.1002/cbic.201800626

One could already exclude the first option (Scheme 2a) by considering the analysis of the composition of the reaction mixture after the biocatalytic reductive amination. In fact, the concentration of amine donor (**b-d**) remained constant at nearly 1 M concentration from the beginning until the end of the reaction. This observation indicates a negligible, if any at all, formation of ammonia during the course of the reaction. On the other hand, our research group as well as other groups have shown that a large excess of ammonia (ca. 0.2-1 M) is required in order to drive the reductive amination of ketone substrates (15-50 mM) in aqueous buffer to a significant extent.[6-8, 10d, 10i] Moreover, AmDHs such as Ch1-AmDH show a K_M value of ca. 1 M for ammonia.[10b] Similarly, with the only exception of the glutamine dehydrogenases from bovine liver, frog liver and *Clostridium* SB_4, the parent wild-type amino acid dehydrogenases are also characterised by elevated K_M values for ammonia (20-500 mM).[20] Consequently, the biocatalytic reductive amination with ammonia is kinetically disfavoured already at significant concentration of ammonia as amine donor. Nonetheless, we investigated this possibility by incubating Rs-AmDH (102.8 μM) with cyclopropylamine (**d**, 50 mM) and NAD^+ (60 mM) in phosphate buffer at pH 8.5, at 30 °C (SI, section 6.1). The possible formation of ammonia was determined indirectly by analytical quantification of the consumption of **d**. As expected, the concentration of **d** remained constant during 48 h hence excluding any detectable formation of ammonia by oxidative deamination of **d** catalysed by Rs-AmDH.

The second option foresees the elimination of an alcohol (Scheme 2b; cyclopropanol in the example) during the possible catalytic cycle of the enzymatic reductive amination between ketones (1 in the example) and amine donor (**d**, cyclopropylamine in the example). By careful monitoring of the reactions, the formation of cyclopropanol as by-product was never

10.1002/cbic.201800626

observed. Analysis was accomplished by comparing the GC-MS chromatogram (*i.e.* retention times and fragmentation patterns) of authentical cyclopropanol as reference compound against the GC-MS chromatograms for the enzymatic reductive amination (for details, see SI section 6.2). Crucially, control experiments also revealed that cyclopropanol (used as reference compound) is stable in the reaction buffer (1M, pH 8.5) at 30 °C and within the 48 h reaction time (SI, section 6.2).

The last option foresees a promiscuous formal transamination via NAD^+/NADH redox-mediated iminium isomerisation (Scheme 2c). Firstly, we ascertained that the presence of the nicotinamide coenzyme was crucial for a possible formal transamination. Hence, Rs-AmDH (102.6 μM) and ketone **1** (10 mM) were incubated in aqueous buffer of amine **d** (1M, pH 8.5), but in absence of NADH. As expected, we did not observe any formation of products (for details, see SI section 6.3). Then, in order to exclude any possible classical transamination reaction that is enabled by pyridoxal 5'-phosphate (PLP) as cofactor, we also repeated the same experiment but in presence of exogenous PLP (0.5 mM). Even in this case, the formation of any product was not observed. Finally, we undertook further experiments for proving the promiscuous enzymatic activity as depicted in Scheme 3c. In the first set of experiments, we incubated chemically synthesised racemic *N*-(1-(4'-fluorophenyl)propan-2-yl)cyclopropanamine (**1d**) in aqueous buffer in presence of NAD^+ (varied concentration from 2 mM to 20 mM) and Rs-AmDH. In this way, we aimed at creating a dynamic equilibrium between all possible oxidative deamination pathways and reductive amination pathways (for schematic details, see SI section 6.4). Crucially, control experiments (*i.e.* without AmDH) showed that **1d** is stable under these reaction conditions and no reaction was observed. In contrast, the incubation of **1d** and NAD^+ with the AmDH

10.1002/cbic.201800626

produced measurable amounts of primary amine **1a** (for details see SI section 6.4, Table S6). The concentration of **1a** detected was typically low (ca. 1% conversion) because **1a** is also in equilibrium with **1** (ca. 7% conversion), the latter species being favoured because of the aqueous environment (schematic details in SI section 6.4). Thus, with these experiments, we proved that the Rs-AmDH converts the secondary amine rac-**1d** into the primary amine (*R*)-**1a**, which is the second part of the mechanism depicted in Scheme 3c. A further experiments of kinetic resolution (SI, section 6.4) on *rac*-**1d** catalysed by Rs-AmDH and using NAD-oxidase (NOx) for NAD^+ recycling was also performed. Detailed analysis of the composition of the reaction mixture revealed that the enzyme is indeed capable of distinguishing between the two enantiomeric forms of **1d**. In fact, the enantiomeric excess of remaining substrate **1d** increased during the time. After 48 h reaction time, the remaining **1d** was ca. 70% whereas its *ee* was ca. 16% (SI, Table S7). If perfect kinetic resolution had occurred, the remaining *ee* should have been instead 30% (*i.e.* 70% remaining **1d** equal to 20% of 1st enantiomer and 50% of 2nd enantiomer; hence theoretical ee = (50-20) = 30%). Thus, these data clearly demonstrate that, albeit one enantiomer of the secondary amine **1d** is preferred, both enantiomers can be accepted by Rs-AmDH.

In conclusion, considering all the results, the side-product formation of enantiopure primary amines is originated by a non-classical promiscuous transamination activity that is mediated by the nicotinamide coenzyme. The expected ketone by-products such as cyclopropanone, or formaldehyde, or acetaldehyde could not be observed because of their known elevated instability and reactivity in solution.

10.1002/cbic.201800626

Elucidation of the stereoselective properties of AmDHs with the aid of computational studies. The models of Rs-AmDH, previously discussed, served as starting point towards a deeper understanding on how a given substrate interacts with the active-site residues of the enzyme while adapting its putative reactive pose(s). This information was used in the subsequent molecular modelling of the Ch1-AmDH described in this paragraph. In fact, for the in-depth computational analysis aimed at elucidating the experimental observations regarding the stereoselectivity of the AmDHs, we selected the reaction between ketone (**1**) and methylamine (**b**), which is catalysed by Ch1-AmDH. This choice was taken because data of conversion and enantiomeric excess for the reaction between **1** and **b** were available (Table 1, entry 1 and 2). Therefore, direct comparison between computational data and experimental laboratory data was possible.

Since the crystal structure of Ch1-AmDH is not publically available, the initial step was to generate a high-quality homology model of this enzyme. The model of Ch1-AmDH was generated in two steps. Firstly, an "exploratory homology modelling run" was executed in order to determine what was (were) the best suitable template(s) for this enzyme. Secondly, a "productive homology modelling run" was executed only considering the "best" template(s) as candidate(s), (for details, see experimental part and SI section 5.2). It is noteworthy that our homology model was created with the enzyme in its reactive conformation (*i.e.* "closed conformation") in which the nicotinamide coenzyme is bound in the active site. That is an important prerequisite for performing molecular docking simulation with these enzymes as described in this work. In contrast, the available crystal structure of opine dehydrogenases (ODHs), which also catalyse the formation of secondary amine functionalities following a formally similar mechanism, are reported in the non-

10.1002/cbic.201800626

reactive conformation ("open conformation") in which the nicotinamide coenzyme is unfortunately absent.[16c]

We initially performed Molecular Docking simulations using the obtained model of Ch1-AmDH as target with the iminium intermediates **1a*** and **1b*** as ligands (*i.e.* **1a*** and **1b*** are generated by the interaction between the ketone **1** with ammonia (**a**) or methylamine (**b**), respectively). The aim was to obtain models of the possible reactive conformations that explain the different stereoselectivity of the reaction, considering the formation of the *R*-configured enantiopure primary amine by reaction of **1** with **a** [10b, 10d] or both secondary amine enantiomers by reaction of **1** with **b**. Through the analysis of the structures obtained with molecular docking simulations, we were able to create the putative pro-*R* and pro-*S* binding modes for both iminium intermediate: **1a*** and **1b***. Comparing the models of Ch1-AmDH possessing **1a*** bound either in pro-*S* or in pro-*R reactive conformation*, the calculated binding energies as well as the calculated distances between the departing hydride of NADH and the prochiral carbon of the iminium intermediate (distance 1 as defined in Figure 2) were similar. A similar scenario was also observed in the models of Ch1-AmDH possessing **1b*** bound either in pro-*S* or in pro-*R reactive conformation*. For this reason, we executed a set of Molecular Dynamics simulations with the aim of "relaxing" the docked enzyme-substrate complexes and, therefore, allowing for a more accurate re-evaluation of the reactive conformations for **1a*** and **1b*** (Figure 3a-b and SI section 5.2 for details). After MD relaxation, it was evident that Ch1-AmDH does not tolerate well **1a*** in the pro-*S* binding mode (see SI section 5.2, Figure S6b and S7b); hence, the pro-*R* binding mode is highly preferred for **1a***. After MD conformational relaxation, the following scenario was observed. Figure 3c and 3d depict: 1) the average relative binding energies for the binding of the imine intermediates (pro-*S* **1a***, pro-*R* **1a***, pro-*S* **1b*** and pro-*R* **1b***) in the active site of Ch1-AmDH; 2) the average distances

10.1002/cbic.201800626

between the departing hydride of NADH and the pro-chiral carbon of the imine intermediates (distance 1 as previously defined). The pro-*S* binding conformation of **1a*** is the less favoured compared to all the other binding conformations (Figure 3c) that appears energetically similar. More instructive is the analysis of the behaviour of the distance 1 over the time of the simulations. The substrate intermediate **1a*** in its pro-*R* conformation showed an average distance 1 of 2.90±0.20 Å, while in its pro-*S* conformation moved considerably above the threshold distance with an average of 3.74±0.64 Å. A slightly similar behaviour was observed for the substrate intermediate **1b***. **1b*** showed an average distance 1 value of 2.69±0.11 Å in its pro-*R* conformation, while it showed a higher average distance value of 3.29±0.36 Å in its pro-*S* conformation. Nevertheless, it is important to note that distance 1 for pro-*S* **1b*** (3.29±0.36 Å) is relatively shorter than the same distance for pro-*S* **1a*** (3.74±0.64 Å). This finding indicates that Ch1-AmDH must tolerate better the pro-*S* conformation of **1b*** than the pro-*S* conformation of **1a***. On the other hand, **1b*** in the pro-*R* orientation is still the preferred binding mode by Ch1-AmDH. That can be observed further in Figure 3d, in which approximately 94% of the MD snapshots (within the simulation time) represent the pro-*R* **1b*** intermediate in the active site of Ch1-AmDH with a distance between its prochiral carbon atom and the attacking hydride of NADH (distance 1 as previously defined) below the threshold of 3 Å (required for hydride shift). Thus, there is an elevated probability that the hydride shift from NADH to **1b*** occurs if **1b*** is bound in its pro-*R* binding conformation. Conversely, the pro-*S* binding conformation of **1b*** is less favourable for hydride shift from NADH because only approximately 32% of the MD snapshots showed a distance 1 below the threshold of 3 Å.

On the other hand, the relative binding energies of **1b*** on pro-*R* and pro-*S* conformations respectively seem to be approximately the same (Figure 3c). We can therefore conclude that,

10.1002/cbic.201800626

although tolerated, the pro-*S* configuration of **1b*** has a lower probability to react than the pro-*R* contra-part. The pro-*S* conformation of **1b*** seems to be stabilised by hydrophobic interactions of the methyl-group with residues M75, A298 and C310. The pro-*R* binding mode of **1b*** is stabilised as already known from literature for wild-type AADHs.[17] This stabilisation involves the previously discussed highly conserved Asp residue (numbering 125 for Ch1-AmDH) in a similar way as depicted in Figure 2 for Rs-AmDH. The described enzyme/substrate contacts for Ch1-AmDH are depicted in Figure 3e-f for both pro-*R* and pro-*S* binding modes. It is interesting to note that the intermediate **1b*** bound in its reactive pro-*R* binding mode was mainly observed assuming the *E* configuration at the C=N double bond (Figure 3a and 3e). In contrast, the intermediate **1b*** bound in its reactive pro-*S* binding mode was mainly observed assuming the *Z* configuration (Figure 3b and 3f). It is known for literature that *N*-alkylimines can isomerise in solution at ambient temperature by tautomerisation and rotation.[21] In the case of intermediate **1b***, which bears non-bulky substituents such as hydrogen or methyl groups, the *E* isomer is known to be favoured in equilibrium in solution at room temperature.[22] Nonetheless, in our case, the enzyme selects the preferred *E* or *Z* configuration of the intermediate in the active site.

10.1002/cbic.201800626

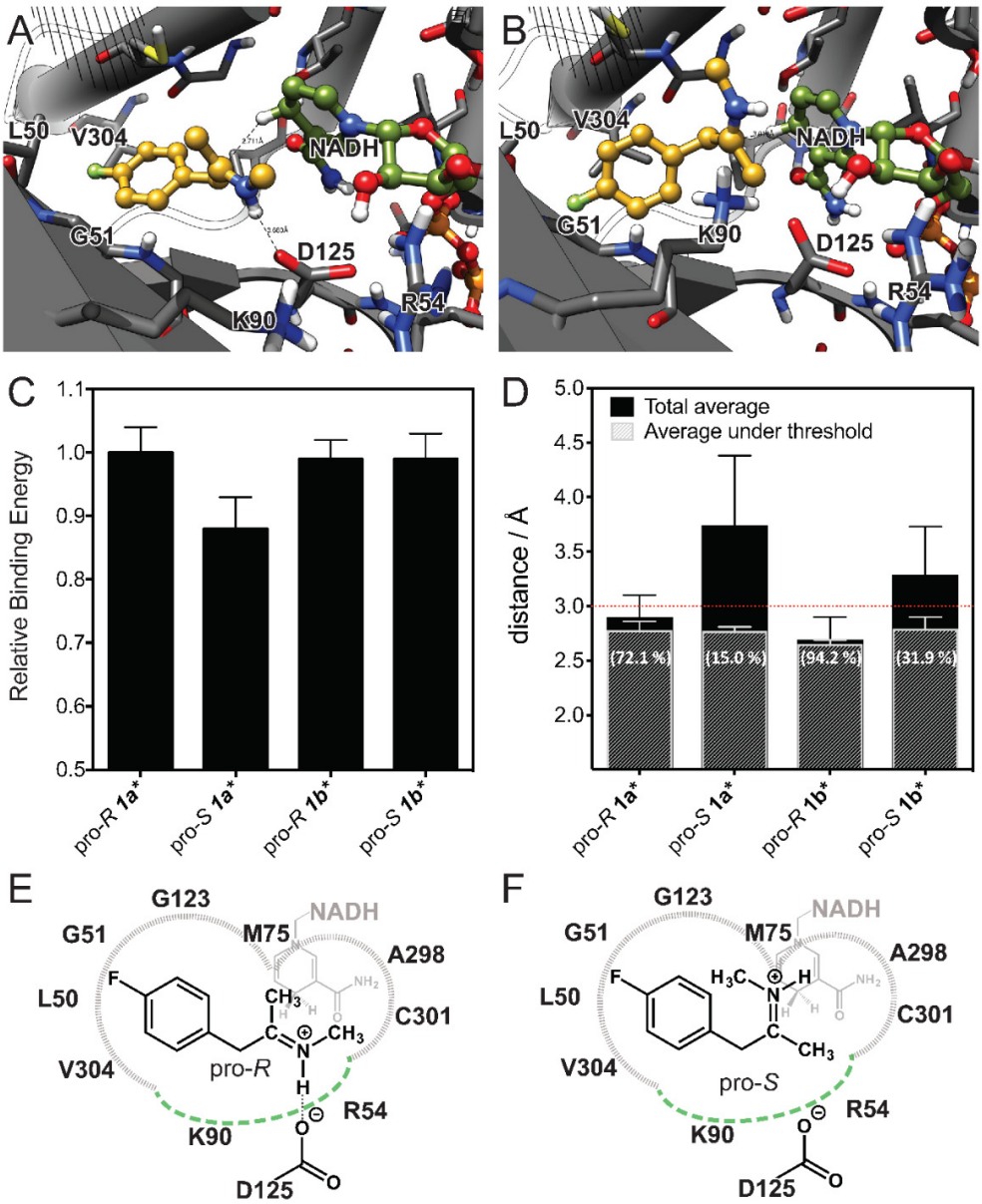

Figure 3. Pro-chiral preferences of Ch1-AmDH. Representative relaxed molecular dynamics snapshots of the **1b*** on its pro-*R* (a) and pro-*S* (b) conformations. The substrate is shown in yellow, while the NADH is shown in green. For clarity, all non-polar hydrogen atoms were not shown. Panel (c) depicts the relative binding energy for **1a*** and **1b*** on their pro-*R* and pro-*S* configuration. All the binding energies are given as relative to the average binding energy of **1a*** on its pro-*R* conformation. **A lower value of relative binding energy means a less favourable binding.** Only those snapshots that showed the substrate on its "*reactive conformation*" were considered for binding energy determination. Panel (d) depicts the distance from the departing hydride of the coenzyme (NADH) to the pro-chiral

10.1002/cbic.201800626

carbon of the ligand (iminium) for **1a*** and **1b*** (in both pro-*R* and pro-*S* configurations). The number in between brackets indicate the percentage of snapshots that contributed with substrates located under the distance threshold (3 Å). Panel (e) and (f) depict the observed enzyme/substrate contacts for **1b*** on its pro-*R* and pro-*S* conformation, respectively. Lines in grey indicate hydrophobic interactions, while the dashed green line indicate hydrophilic interactions. The NADH cofactor is depicted behind the substrate in light-grey.

Additionally, a non-bonding dihedral angle (χ) was defined in order to describe the stereo-binding mode of the substrate in the active site (Figure 4a). This dihedral angle was defined following the Cahn–Ingold–Prelog priority rules between the three atoms bonded to the pro-chiral carbon of the substrate and the hydride atom of the NADH cofactor. This dihedral angle was determined for the *R*- and *S*- configured products (both for **1a** and **1b**) of the reaction, indicating that the *R*-configured product shows an average value of 63.85±0.20°, while the *S*-configured product shows an average value of -63.95±0.27°. Figure 4b shows the behaviour of the χ angle in function of the time for substrate intermediates **1a*** and **1b*** and starting from both pro-*R* and pro-*S* binding conformations. Notably, in the case where the intermediate substrate **1a*** is bound in a pro-*S* binding mode, a switch to the pro-*R* conformation occurred within the simulation time (Figure 5b; for details see SI section 5.2 and Figure S7b; see also SI movie file "switch_pro-S_to_pro-R_primary_imine.avi"). In particular, 50% of the simulation runs for pro-*S* **1a*** (3 out of 6) showed this switch from pro-*S* to pro-*R* (Figure 5b, black line). An additional simulation (run 5) also showed a switch in the conformation but, during this simulation, the substrate moved out of the active-site. Therefore, we did not consider this simulation into the calculation of the average values. Only in 2 cases out of 6, substrate **1a*** maintained the pro-*S* binding conformation (Figure 5b, green line). In contrast to the simulation with pro-

10.1002/cbic.201800626

S **1a***, a conformational switch was never observed for simulations starting from either pro-*R* **1a*** or pro-*R* **1b***or pro-*S* **1b*** (Figure 4; for details see SI section 5.2 and Figure S7a,c,d). It is important to remark that the average value of the herein defined dihedral angle for pro-*S* **1a*** amongst simulation runs has only illustrative value, thus indicating great conformational changes in the active site of Ch1-AmDH.

In summary, the molecular dynamic simulations provide an insight at molecular level on the different stereoselective behaviour of the AmDHs in the reductive amination of prochiral ketones with either ammonia or more complex amines. When ammonia is the amine donor, the *reactive* pro-*R* conformation of the iminium intermediate is much more favoured than the pro-*S* conformation explaining why the primary amine product is always experimentally obtained in enantiopure *R*-configured form.[10d] In the event that a pro-*S* binding mode for the primary iminium intermediate is generated in the active site, a conformational switch to pro-*R* binding mode (Figure 4B; see also SI movie file "switch_pro-S_to_pro-R_primary_imine.avi") or even the release of the intermediate from the active site is likely to occur. Conversely, when a primary amine is the amine donor for the reductive amination, both pro-*R* and pro-*S* binding modes can be generated as reactive conformations so that the secondary amine product is obtained in both enantiomeric forms.

10.1002/cbic.201800626

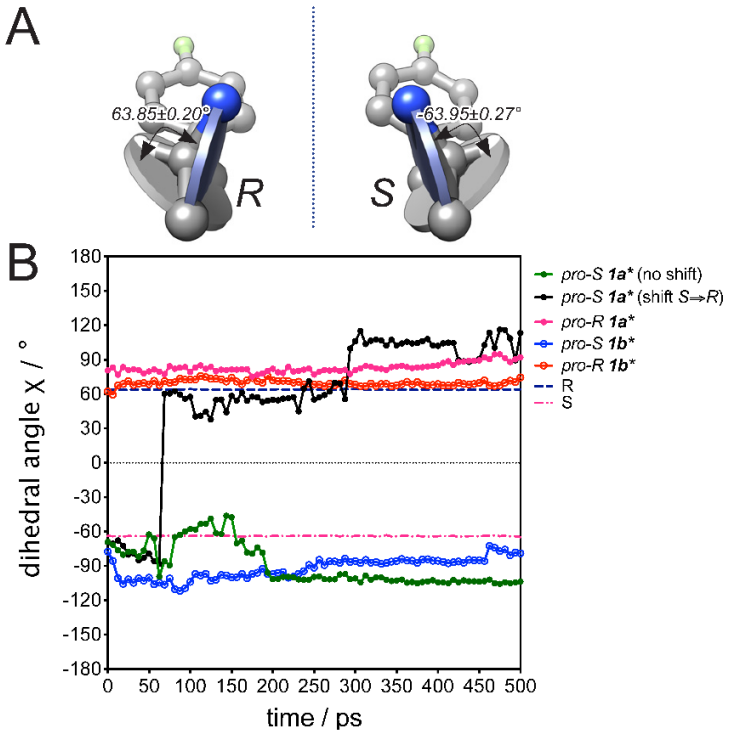

Figure 4. Dihedral angle χ versus time for the Molecular Dynamics Simulations starting from pro-*R* **1a***, pro-*S* **1a***, pro-*R* **1b*** and pro-*S* **1b***. (a) Illustrative depiction of the χ angle for the *R*- and *S*-configured product of the reaction. These values were used as reference for describing the hydride shift from NADH that would afford any of these enantiomers. According to this definition, a positive value of the dihedral angle in the intermediate will lead to the *R*-configured amine upon reduction. A negative value will lead to the *S*-configured amine upon reduction. (b) The average variation of χ angle over the time is shown for the simulations of pro-*R* **1a*** (purple), pro-*S* **1a*** (black or green), pro-*R* **1b*** (orange) and pro-*S* **1b*** (blue). For each system, the depicted line is the average of six independent simulation runs (all simulation runs are reported in the SI, Figure S7). Only the simulation run number 5 for substrate **1a*** in pro-*S* binding conformation was not considered for the average calculation due to fact that the substrate moved away from the active site (for details, see SI, Figure S7b). For the sake of clarity of the depiction, the error-bars of these average simulations have been omitted (for this detailed information see SI Figure S7). The average χ values for the *R*-configured (blue) and *S*-configured products (purple) are also shown as dashed lines.

10.1002/cbic.201800626

Proposed catalytic mechanism. Considering all the results obtained from practical experimental laboratory and computational experiments, we postulated a biocatalytic cycle that illustrates the formation of both secondary and primary amines (Scheme 3). The proposed cycle is adapted from the catalytic mechanism of the phenylalanine dehydrogenases from *Rhodococcus sp.* M4 (the wild-type parent of the variant Rs-AmDH).[17]

In the first step, the carbonyl compound and the amine donor generate the geminal amino alcohol (**I** or **I'**) assisted by a protonated Lys and a deprotonated Asp residues from the AmDH active site. Intermediate **I** and **I'** can interconvert through a rotation around the carbon-carbon bond that connects the prochiral C-sp^2 of the ketone and the C-sp^3 in its α-position (the latter connected to substituent R^1 in Scheme 3). This rotation appears to be the most probable one since our model structures clearly show that the R^1 substituent (e.g. in this study phenyl, phenylmethyl, alkyl) is tightly accommodated in a hydrophobic cavity in the active site of the AmDH (Figure 5).

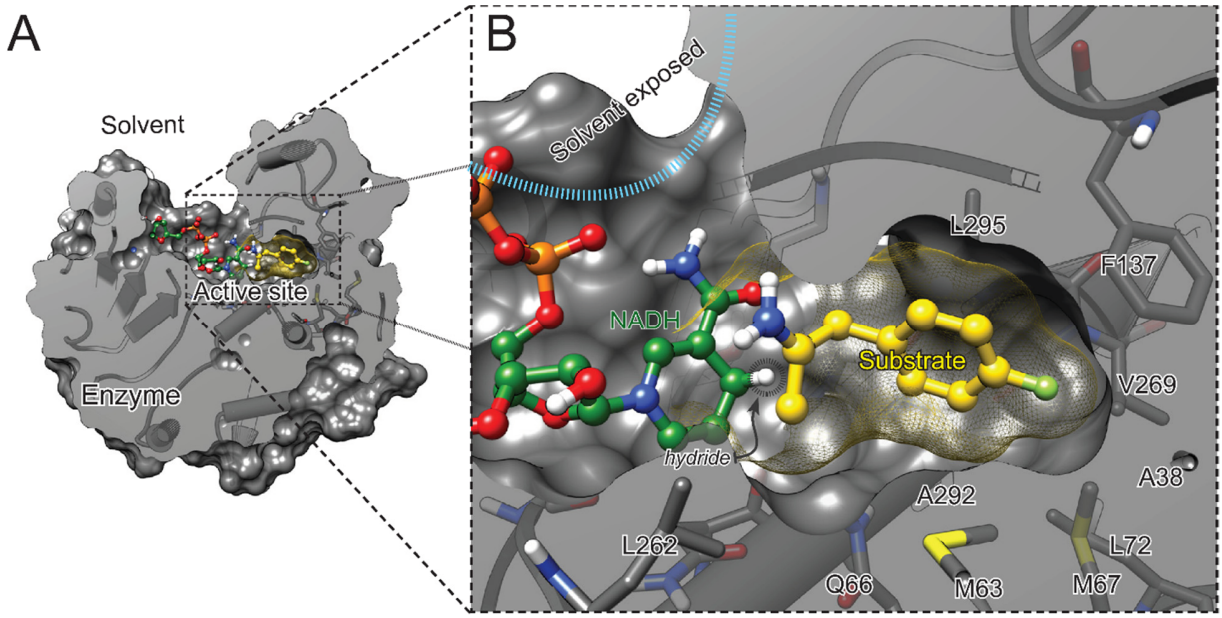

10.1002/cbic.201800626

Figure 5. (a) Hydrophobic binding pocket of RsAmDH (b) Amino acid residues constituting the hydrophobic binding pocket in the active site of Rs AmDH

Then, assisted by the same Lys residues, a water molecule is released from intermediate **I** or **I'** to generate the iminium intermediate **II** (pro-*R* binding mode) and **II'** (pro-*S* binding mode), respectively. From the analysis of the snapshots of our molecular docking simulations, it appears that the iminium moiety of the intermediate **II** (pro-*R*) is stabilised further by a hydrogen bond with the deprotonated aspartate residue (Figures 3a and 3e; Asp 118 in Rs-AmDH or Asp 125 in Ch1-AmDH). In contrast, such a hydrogen bond was not observed with intermediate **II'** since the aspartate residue is too distant from the hydrogen of the iminium moiety. Intermediate **II'** appears to be stabilised by hydrophobic interactions of the methyl group with residues M75, A298, C310 (Figure 3b and 3f). As observed before, intermediate **II** assume the preferred *E* configuration whereas intermediate **II'** assumes the preferred *Z* configuration (in Scheme 3, C.I.P. priority: $R^1 > R^2$). Although a conformational switch from pro-*S* to pro-*R* binding mode (or vice versa) of the secondary imine intermediate was never observed within the time of our simulations, this event can not be completely ruled out. Hence, this theoretically possible conformational binding switch was depicted as dashed line in Scheme 3. In contrast, as previously described, such a conformational binding switch from pro-*S* to pro-*R* (but not vice versa) is very likely to occur with primary iminium intermediates (Figure 4b; see also SI movie file "switch_pro-S_to_pro-R_primary_imine.avi").

At this stage, hydride shift from NADH to intermediate **II** or **II'** can occur to furnish the secondary amine product in *R*-configuration or *S*-configuration, respectively. Nonetheless, the amine (*R*)-**1b** obtained by reduction of intermediate **II** can be also subjected to a further promiscuous re-oxidation in the active site by abstraction of the hydride from the other alkyl chain of the amine

10.1002/cbic.201800626

moiety. This promiscuous formal imine isomerisation generates intermediate **III**. Hydrolysis of intermediate **III** by the same water molecule coordinated to the catalytic Lys residue or by another polarised water molecule at proper distance in the active site forms the primary amine product (*R*)-**1b** as single enantiomer.

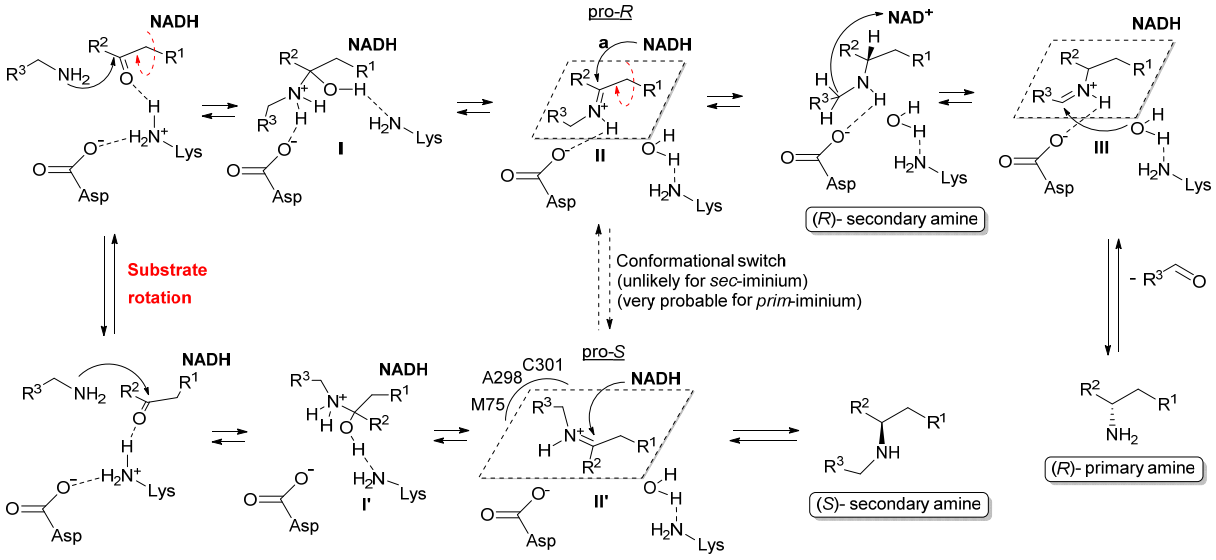

Scheme 3. Proposed catalytic cycle for the reductive amination catalysed by Rs-AmDH and Ch1-AmDH with amine donors different from ammonia (adapted from reference 17). Two stereocomplementary binding modes are the most probable: either intermediate **II** (*E* configuration and pro-*R* binding mode) or intermediate **II'** (*Z* configuration and pro-*S* binding mode). Interconversion between **II** and **II'** (and vice versa) was never observed for secondary iminium intermediates during the time of our simulations. In contrast, interconversion from **II'** to **II** was observed in 50% of the cases in our simulations with primary iminium intermediates. The opposite interconversion (from **II** to **II'**) was never observed. Further reduction of intermediate **II'** by hydride shift from NADH forms the secondary amine product in *S*-configuration. Reduction of intermediate **II** by hydride shift from NADH forms the secondary amine product in *R*-configuration. However, intermediate **II** can also be re-oxidised to the iminium isomer **III**. After this formal imine isomerisation step, the hydrolysis of intermediate **III** furnishes the primary amine product in *R*-configuration.

Conclusions

10.1002/cbic.201800626

The known AmDHs were engineered from amino acid dehydrogenases and therefore they display the highest catalytic activity with ammonia as amine donor. In contrast to the common belief that ammonia is the only possible amine donor, we have demonstrated in this work that the reactivity of AmDHs can be extended to other amine donors. In fact, enantioenriched secondary amines were obtained with conversion up to 43%. However, we observed that the control of the chemo- and stereoselectivity of the reductive amination catalysed by AmDHs with different amine donors is challenging. This study revealed that the secondary amine products can be obtained just in enantioenriched form, so far. Furthermore, an unprecedented nicotinamide (NAD)-dependent isomerisation step may take place in the active site of the enzyme, during the catalytic cycle, ultimately leading to the formation of the structurally related enantiopure primary amine as additional product. To the best of our knowledge, our findings suggest the first example of a formal enzymatic transamination mechanism that is not catalysed by PLP. By combining practical laboratory experiments and computational experiments and analysis, we could rationalise the formation of all the products observed in the reaction mixture. Finally, a catalytic cycle was postulated based on the known natural catalytic cycle of the wild-type phenylalanine dehydrogenases from *Rhodococcus sp.* M4.

In summary, this study provides an understanding of the molecular discriminants that are crucial for the efficient catalytic activity of AmDHs, and it will contribute to provide the knowledge required for further rational engineering of AmDHs in order to improve activity, stereoselectivity and suppress possible side-reactions.

10.1002/cbic.201800626

Experimental

For general information, materials, details on computational molecular modelling, chemical synthesis of references compounds and analytics, see Supporting Information.

General procedure for the biocatalytic amination of carbonyl compounds 1-13 with amine donors b-j.

All buffers were prepared by mixing each amine donor **b-k** (See Figure S2) with distilled water to obtain a final concentration of 1 M. The pH was adjusted to 8.5 with formic acid. In the case of aniline (**l**), due to solubility issues, saturated solution of aniline (pH 8.5) was used. Both amine dehydrogenases (Rs-AmDH and Ch1-AmDH) were tested for the synthesis of secondary or tertiary amines by using all eleven different amine buffers, as well as the carbonyl compounds **1-12** as acceptor substrates (for detailed structures, see SI, Figure S1).

Biotransformations were performed in 1.5 mL Eppendorf tubes with a total reaction volume of 0.5 mL. The reaction consisted of NAD^+ (1 mM), substrate (10 mM), AmDH (102.8 µM for Rs-AmDH and 91.8 µM for Ch1-AmDH) and Cb-FDH (23.5 µM). Reactions were performed at 30 °C for 48 h on orbital shakers (170 rpm) in a horizontal position. The reactions were quenched after 48 h by the addition of aqueous KOH (10 M, 100 µL). Then, the organic compounds were extracted with dichloromethane (CH_2Cl_2, 1 x 600 µL) and dried with magnesium sulphate. The conversions were measured by GC-FID using commercially available or chemically synthesised reference compounds. In the cases where reference compounds were not available, preliminary identification of the desired products (amines) was also done by GC-MS using the same column and method as for GC-FID. The enantiomeric excess was determined after derivatization to acetamido using a solution of DMAP (50 mg) in 1 mL of acetic anhydride (409 mM). In total, 50 µL of this solution

10.1002/cbic.201800626

was added to each 600 µL dichloromethane contained the amine product. The mixtures were shaken at 25 ºC for 30 min. After that 500 µL of water was added for another 30 min with shaking at 25 °C. The samples were centrifuged for 10 min at 14800 rpm and the organic phases were dried with magnesium sulphate prior to the injection in the Chrompack Chiracel Dex-CB (25 m, 320 µm, 0.25 µm, Agilent), or Hydrodex-β-TBDAC (50m, 0.40 mm, 0.25 mm, Macherey-Nagel).

Computational molecular modeling

Computational model of Rs-AmDH

The 3D structural model of Rs-AmDH was created starting from the crystal structure of the L-phenylalanine dehydrogenase from *Rhodococcus sp.* M4 (PDB code: 1C1D).[17] The Rs-AmDH variant differs only for three amino acids positions from the wild-type L-phenylalanine dehydrogenase: namely K66Q, S149G, and N262C.[7] These mutations were *in silico* induced using the Yasara software,[23] utilising the AMBER 03 force field.[24] The protonation state of all atoms was automatically adjusted, with the exception of those atoms involved in the hydride transfer between the co-factor and the substrate. The protonation state of the latter atoms was adjusted manually accordingly. Every time a mutation was induced a three-step energy minimization was executed. Step one: only the mutated residue was energetically minimized. Step two: the mutated residue plus all those residues within a radius of 6 Å from the mutated residue were subjected to energy minimization. Step three: the complete enzyme was submitted to energy minimization. By using this energy minimization protocol, it was assured a gradual adjustment of the complete structure to the new mutation, thus avoiding the production of undesired deformations of the secondary structure.

10.1002/cbic.201800626

All selected substrates were generated *in situ* by mimicking the observed position of L-phenylalanine in the crystal structure PDB 1C1D. After substrate generation, the three-steps energy minimization protocol above-described was applied. These models were created for studying the possible reactive poses of Rs-AmDH containing the ketimine (SI, Figure S4) and aldimine (SI, Figure S5) intermediates formed during the catalytic mechanism. Based on the reported catalytic mechanism of the parent wild-type L-phenylalanine dehydrogenase from Rhodococcus sp. M4[17], we analysed the models considering two crucial parameters*:* 1) the distance between the attacking hydride of NADH and the pro-chiral carbon of the iminium intermediate (distance 1); 2) the distance between the negatively charged oxygen atom of the terminal carboxylic group of D118 in Rs-AmDH and the hydrogen of the iminium group (distance 2). For details and figures, see SI section 5.1.

Computational model of Ch1-AmDH

Ch1-AmDH chimeric enzyme was previously created in laboratory by domain shuffling of two first generation variants such as Bb-PhAmDH (originated from *Bacillus badius* L-phenylalanine dehydrogenase) and L-AmDH (originated from *Bacillus stearothermophilus* L-leucine dehydrogenase).[10b] The Ch1-AmDH model structure was generated in two steps. Firstly, an "exploratory homology modelling run" was executed in order to determine what was (were) the best suitable template(s) for this enzyme. Then, a second homology modelling run was executed only considering the "best" template(s) as candidate(s).

Exploratory homology modelling run. This exploratory run was carried out using the YASARA [23] homology model building protocol,[25] which involves multi-template structural model generation. Since the linear amino acid sequence of the target protein was the only given input, the possible templates were identified by running 3 PSI-BLAST[26] iterations to extract a position

10.1002/cbic.201800626

specific scoring matrix (PSSM) from UniRef90,[27] and then searching the PDB for a match with an E-value below the homology modelling cut-off of 0.005. A maximum of 5 templates was allowed. To aid alignment correction and loop modelling, a secondary structure prediction for the target sequence had to be obtained. This was achieved by running PSI-BLAST to create a target sequence profile and feeding it to the PSI-Pred[28] secondary structure prediction algorithm. For each of the found templates, models were built. Either a single model per template was generated, when the alignment was certain, or a number of alternative models were generated, when the alignment was ambiguous. A maximum of 50 conformations per loop were explored. A maximum of 10 residues were added to the termini. Finally, YASARA attempted to combine the best parts of the generated models to obtain a hybrid model, with the intention of increasing the accuracy beyond each of the contributors. The quality of the models was evaluated by the use of Z-score[29]. A Z-score describes how many standard deviations the model quality is away from the average high-resolution X-ray structure. The overall Z-scores for all models have been calculated as the weighted averages of the individual Z-scores using the formula: Overall = 0.145*Dihedrals + 0.390*Packing1D + 0.465*Packing3D. The overall score thus captures the correctness of backbone- (Ramachandran plot) and side-chain dihedrals, as well as packing interactions.

Production homology modelling run. Based on the results of the exploratory run, it turned out that the generated model showed a reasonably good quality; however, it contained neither the cofactor nor a co-crystalized substrate in its active-site. For this reason, the template 1C1D was only considered for the production run. In fact, the crystal structure of 1C1D was co-crystalized with cofactor and substrate in its active-site.[17] In summary, the production run was carried out using the same parameters used in the exploratory run with exception of the following parameters: only one template was manually selected, a maximum of 100 conformations per loop were explored

10.1002/cbic.201800626

and a maximum of 2 residues were added to the termini. In order to increase their quality, the obtained models were submitted to 500 picoseconds molecular dynamic refinement simulation using the protocol describe by E. Krieger et al.[30]. A structural snapshot was saved every 25 picoseconds for further analysis of quality parameters (potential energy, Dihedrals, Packing1D and Packing3D). The model with the best quality was selected for further computational molecular studies. In Supporting Information section 5.2 (Table S4), the results of homology model generation are reported.

Computational molecular docking and molecular dynamics simulations

The model of Ch1-AmDH obtained in the previous step was used as starting point for the molecular dynamics (MD) simulations. MD simulations were executed using the Yasara software,[23] with the AMBER 03 force field.[24] Prior to this, all substrates were *in situ* generated starting from the reactive pose of *L*-phenylalanine. After substrate generation, the three-step energy minimization protocol was applied. These models were created representing the reactive pose of Ch1-AmDH with the iminium intermediate. The final relaxed structure was evaluated using the Autodock Vina[31] scoring function in order to assess its binding energy at its reactive pose. Both binding conformations, pro-*R* and pro-*S* obtained, were submitted to MD simulations. A minimum of six independent MD simulations (with random initial velocities) were executed per system. Each MD simulation was run for 500 ps, and a snapshot was taken every 6.25 ps, thus resulting in 81 frames (counting the starting structure) per simulation. These frames were submitted for analysis and several dynamic properties were followed. However, the distance between the departing hydride of NADH and the pro-chiral carbon atom of the imine intermediate substrate was considered as the main descriptor of the reactive pose. The sum of the van der Waal's radius [18] of carbon and

hydrogen was considered as the threshold distance, which was set to a rounded value of 3.0 Å ($r_H^{vdw} = 1.2$ Å, $r_C^{vdw} = 1.7$ Å; $r_H^{vdw} + r_C^{vdw} = 2.9$ Å; thus: $d_{CH}^{threshold} = 3.0$ Å).

Acknowledgements

This project has received funding from the European Research Council (ERC) under the European Union's Horizon 2020 research and innovation programme (grant agreement No 638271, BioSusAmin). Dutch funding from the NWO Sector Plan for Physics and Chemistry is also acknowledged. The authors thank Dr. Hans Iding (Hoffmann-La Roche Ltd.) for his high valuable contribution towards the understanding of the catalytic pathway that explains the promiscuous NAD-dependent formal transamination activity as described in this article.

Conflict of interest

The authors declare no conflict of interest.

Keywords:

reductive amination, enzyme promiscuity, α-chiral amines, biocatalysis, amine dehydrogenases, transamination

Notes and references

[1] a) O. Khersonsky, D. S. Tawfik, *Annu. Rev. Biochem* **2010**, *79*, 471-505; b) I. Nobeli, A. D. Favia, J. M. Thornton, *Nat. Biotechnol.* **2009**, *27*, 157-167; c) M. S. Humble, P. Berglund, *Eur. J. Org. Chem.* **2011**, *2011*, 3391-3401; d) K. Hult, P. Berglund, *Trends Biotechnol.* **2007**, *25*, 231-238; e) O. Khersonsky, C. Roodveldt, D. S. Tawfik, *Curr. Opin. Chem. Biol.* **2006**, *10*, 498-508; f) U. T. Bornscheuer, R. J. Kazlauskas, *Angew. Chem. Int. Ed.* **2004**, *43*, 6032-6040; g) A. Babtie, N. Tokuriki, F. Hollfelder, *Curr. Opin. Chem. Biol.* **2010**, *14*, 200-207; h) R. J. Kazlauskas, *Curr. Opin. Chem. Biol.* **2005**, *9*, 195-201.

[2] a) J. Vilím, T. Knaus, F. Mutti, *Angew. Chem. Int. Ed.* **2018**, *57*, 14240-14244; b) M. A. Emmanuel, N. R. Greenberg, D. G. Oblinsky, T. K. Hyster, *Nature* **2016**, *540*, 414-417; c) B. A. Sandoval, A. J. Meichan, T. K. Hyster, *J. Am. Chem. Soc.* **2017**, *139*, 11313-

11316; d) X. Garrabou, T. Beck, D. Hilvert, *Angew. Chem. Int. Ed.* **2015**, *54*, 5609-5612; e) A. Cuetos, M. Garcia-Ramos, E. M. Fischereder, A. Diaz-Rodriguez, G. Grogan, V. Gotor, W. Kroutil, I. Lavandera, *Angew. Chem. Int. Ed.* **2016**, *55*, 3144-3147; f) D. Wetzl, J. Bolsinger, B. M. Nestl, B. Hauer, *ChemCatChem* **2016**, *8*, 1361-1366; g) Z. Liu, Y. Lv, A. Zhu, Z. An, *ACS Macro Letters* **2017**, *7*, 1-6; h) S. E. Payer, X. Sheng, H. Pollak, C. Wuensch, G. Steinkellner, F. Himo, S. M. Glueck, K. Faber, *Adv. Synth. Catal.* **2017**, *359*, 2066-2075; i) P. S. Coelho, E. M. Brustad, A. Kannan, F. H. Arnold, *Science* **2013**, *339*, 307-310; j) G. D. Roiban, M. T. Reetz, *Angew. Chem. Int. Ed.* **2013**, *52*, 5439-5440; k) Y. Miao, E. M. Geertsema, P. G. Tepper, E. Zandvoort, G. J. Poelarends, *ChemBioChem* **2013**, *14*, 191-194; l) C. Wuensch, J. Gross, G. Steinkellner, K. Gruber, S. M. Glueck, K. Faber, *Angew. Chem. Int. Ed.* **2013**, *52*, 2293-2297; m) T. Devamani, A. M. Rauwerdink, M. Lunzer, B. J. Jones, J. L. Mooney, M. A. Tan, Z. J. Zhang, J. H. Xu, A. M. Dean, R. J. Kazlauskas, *J. Am. Chem. Soc.* **2016**, *138*, 1046-1056; n) Y. Miao, R. Metzner, Y. Asano, *ChemBioChem* **2017**, *18*, 451-454; o) S. Roth, A. Prag, C. Wechsler, M. Marolt, S. Ferlaino, S. Ludeke, N. Sandon, D. Wetzl, H. Iding, B. Wirz, M. Muller, *ChemBioChem* **2017**, *18*, 1703-1706.

[3] M. J. Abrahamson, E. Vazquez-Figueroa, N. B. Woodall, J. C. Moore, A. S. Bommarius, *Angew. Chem. Int. Ed.* **2012**, *51*, 3969-3972.

[4] F.-F. Chen, Y.-Y. Liu, G.-W. Zheng, J.-H. Xu, *ChemCatChem* **2015**, *7*, 3838-3841.

[5] F.-F. Chen, G.-W. Zheng, L. Liu, H. Li, Q. Chen, F.-L. Li, C.-X. Li, J.-H. Xu, *ACS Catal.* **2018**, *8*, 2622-2628.

[6] M. J. Abrahamson, J. W. Wong, A. S. Bommarius, *Adv. Synth. Catal.* **2013**, *355*, 1780-1786.

[7] L. J. Ye, H. H. Toh, Y. Yang, J. P. Adams, R. Snajdrova, Z. Li, *ACS Catal.* **2015**, *5*, 1119-1122.

[8] A. Pushpanath, E. Siirola, A. Bornadel, D. Woodlock, U. Schell, *ACS Catal.* **2017**, *7*, 3204-3209.

[9] O. Mayol, S. David, E. Darii, A. Debard, A. Mariage, V. Pellouin, J.-L. Petit, M. Salanoubat, V. de Berardinis, A. Zaparucha, C. Vergne-Vaxelaire, *Catal. Sci. Technol.* **2016**, *6*, 7421-7428.

[10] a) S. K. Au, B. R. Bommarius, A. S. Bommarius, *ACS Catal.* **2014**, *4*, 4021-4026; b) B. R. Bommarius, M. Schürmann, A. S. Bommarius, *Chem. Commun.* **2014** *50*, 14953-14955; c) F. G. Mutti, T. Knaus, N. S. Scrutton, M. Breuer, N. J. Turner, *Science* **2015**, *349*, 1525-1529; d) T. Knaus, W. Böhmer, F. G. Mutti, *Green Chem.* **2017**, *19*, 453-463; e) J. Liu, B. Q. W. Pang, J. P. Adams, R. Snajdrova, Z. Li, *ChemCatChem* **2017**, *9*, 425-431; f) T. Knaus, L. Cariati, M. F. Masman, F. G. Mutti, *Org. Biomol. Chem.* **2017**, *15*, 8313-8325; g) H. Ren, Y. Zhang, J. Su, P. Lin, B. Wang, B. Fang, S. Wang, *J. Biotechnol.* **2017**, *241*, 33-41; h) M. P. Thompson, N. J. Turner, *ChemCatChem* **2017**, *9*, 3833-3836; i) W. Böhmer, T. Knaus, F. G. Mutti, *ChemCatChem* **2018**, *10*, 731-735; j) J. Lowe, A. A. Ingram, H. Gröger, *Bioorg. Med. Chem.* **2017**, 26, 1387-1392.

[11] a) J. H. Schrittwieser, S. Velikogne, W. Kroutil, *Adv. Synth. Catal.* **2015**, *357*, 1655-1685; b) M. Sharma, J. Mangas-Sanchez, N. J. Turner, G. Grogan, *Adv. Synth. Catal.* **2017**, *359*, 2011-2025.

[12] a) P. N. Scheller, M. Lenz, S. C. Hammer, B. Hauer, B. M. Nestl, *ChemCatChem* **2015**, *7*, 3239-3242; b) T. Huber, L. Schneider, A. Präg, S. Gerhardt, O. Einsle, M. Müller, *ChemCatChem* **2014**, *6*, 2248-2252; c) D. Wetzl, M. Gand, A. Ross, H. Müller, P.

Matzel, S. P. Hanlon, M. Müller, B. Wirz, M. Höhne, H. Iding, *ChemCatChem* **2016**, *8*, 2023-2026; d) P. Matzel, M. Gand, M. Höhne, *Green Chem.* **2017**, *19*, 385-389.

[13] a) G. A. Aleku, S. P. France, H. Man, J. Mangas-Sanchez, S. L. Montgomery, M. Sharma, F. Leipold, S. Hussain, G. Grogan, N. J. Turner, *Nat. Chem.* **2017**, *9*, 961-969; b) S. L. Montgomery, J. Mangas-Sanchez, M. P. Thompson, G. A. Aleku, B. Dominguez, N. J. Turner, *Angew. Chem. Int. Ed.* **2017**, *56*, 10491-10494.

[14] S. P. France, R. M. Howard, J. Steflik, N. J. Weise, J. Mangas-Sanchez, S. L. Montgomery, R. Crook, R. Kumar, N. J. Turner, *ChemCatChem* **2018**, *10*, 510-514.

[15] Codexis-INC, H. Chen, J. C. Moore, S. J. Collier, D. Smith, J. Nazor, G. Hughes, J. Janey, G. Huisman, S. Novick, N. Agard, O. Alvizo, G. Cope, W.-L. Yeo, J. Sukumaran, S. Ng, **2013**, WO2013/170050.

[16] a) Y. Asano, K. Yamaguchi, K. Kondo, *J. Bacteriol.* **1989**, *171*, 4466-4471; b) Y. Kato, H. Yamada, Y. Asano, *J. Mol. Catal. B: Enzym.* **1996**, *1*, 151-160; c) Y. A. K.L. Britton, D.W. Rice, *Nat. Struct. Biol.* **1998**, *5*, 593-601.

[17] N. M. W. Brunhuber, J. B. Thoden, J. S. Blanchard, J. L. Vanhooke, *Biochemistry* **2000**, *39*, 9174-9187.

[18] R. S. Rowland, R. Taylor, *J. Phys. Chem.* **1996**, *100*, 7384-7391.

[19] a) S. Mathew, H. Yun, *ACS Catal.* **2012**, *2*, 993-1001; b) E. F. Oliveira, N. M. Cerqueira, P. A. Fernandes, M. J. Ramos, *J. Am. Chem. Soc.* **2011**, *133*, 15496-15505; c) P. K. Mehta, T. I. Hale, P. Christen, *Eur. J. Biochem.* **1993**, *214*, 549-561; d) B.-Y. Hwang, B.-K. Cho, H. Yun, K. Koteshwar, B.-G. Kim, *J. Mol. Catal. B: Enzym.* **2005**, *37*, 47-55.

[20] K. S. Toshihisa Ohshima, *Adv. Biochem. Eng./Biotechnol.* **1990**, *42*, 187-209.

[21] a) W. B. Jennings, D. R. Boyd, *J. Am. Chem. Soc.* **1972**, *94*, 7187-7188; b) J. E. Johnson, N. M. Morales, A. M. Gorczyca, D. D. Dolliver, M. A. McAllister, *J. Org. Chem.* **2001**, *66*, 7979-7985.

[22] J. Bjørgo, D. R. Boyd, C. G. Watson, W. B. Jennings, *J. Chem. Soc., Perkin Trans. 2* **1974**, 757-762.

[23] E. Krieger, G. Koraimann, G. Vriend, *Proteins* **2002**, *47*, 393-402.

[24] C. Oostenbrink, A. Villa, A. E. Mark, W. F. van Gunsteren, *J. Comput. Chem.* **2004**, *25*, 1656-1676.

[25] a) E. Krieger, S. B. Nabuurs, G. Vriend, *Methods Biochem. Anal.* **2003**, *44*, 509-523; b) H. Venselaar, R. P. Joosten, B. Vroling, C. A. B. Baakman, M. L. Hekkelman, E. Krieger, G. Vriend, *Eur. Biophys. J.* **2010**, *39*, 551-563.

[26] S. F. Altschul, T. L. Madden, A. A. Schäffer, J. Zhang, Z. Zhang, W. Miller, D. J. Lipman, *Nucleic Acids Res.* **1997**, *25*, 3389-3402.

[27] B. E. Suzek, H. Huang, P. McGarvey, R. Mazumder, C. H. Wu, *Bioinformatics* **2007**, *23*, 1282-1288.

[28] D. T. Jones, *J. Mol. Biol.* **1999**, *292*, 195-202.

[29] a) R. A. Laskowski, M. W. MacArthur, D. S. Moss, J. M. Thornton, *J. Appl. Crystallogr.* **1993**, 283-291; b) R. W. Hooft, G. Vriend, C. Sander, E. E. Abola, *Nature* **1996**, *381*, 272-272.

[30] E. Krieger, T. Darden, S. B. Nabuurs, A. Finkelstein, G. Vriend, *Proteins* **2004**, *57*, 678-683.

[31] O. Trott, A. J. Olson, *J. Comput. Chem.* **2010**, *25*, 1656-1676.

10.1002/cbic.201800626

1 TOC

FULL PAPER

Biocatalytic reductive amination: The catalytic promiscuity of amine dehydrogenases enables the synthesis of enantioenriched secondary and tertiary amines. Along with the expected formation of secondary amines, the promiscuous formation of enantiopure primary amines was observed in several cases. By conducting practical laboratory and computational experiments, we propose a catalytic cycle that explains these findings.

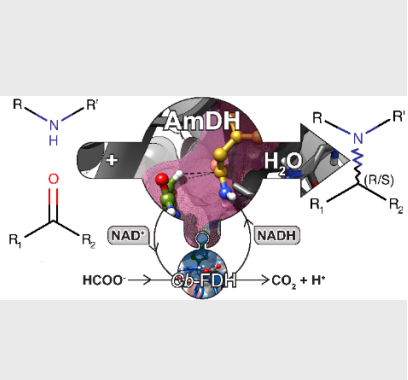

*MSc V. Tseliou, Dr. M. F. Masman, MSc. W. Böhmer, Dr. T. Knaus and Ass. Prof. Dr. F. G. Mutti**

Page No. – Page No.

Mechanistic Insight into the Catalytic Promiscuity of Amine Dehydrogenases: Asymmetric Synthesis of Secondary and Primary Amines

2